



Article

Microstructural Modification of Cold-Sprayed Ti-Cr₃C₂ Composite Coating by Laser Remelting

Vladislav S. Shikalov¹, Diana A. Katanaeva², Tomila M. Vidyuk¹, Alexander A. Golyshev³, Vladimir F. Kosarev¹, Elena E. Kornienko⁴, Alexander G. Malikov³ and Victor V. Atuchin^{5,6,7,8,*}

- ¹ Laboratory of Multiphase Media Physics, Khristianovich Institute of Theoretical and Applied Mechanics, SB RAS, Novosibirsk 630090, Russia; v.shikalov@gmail.com (V.S.S.); tomilka.v@gmail.com (T.M.V.); vkos@itam.nsc.ru (V.F.K.)
 - ² Institute of New Materials and Nanotechnologies, NUST MISIS, Moscow 119049, Russia; dianakat2001@mail.ru
 - ³ Laboratory of Laser Technologies, Khristianovich Institute of Theoretical and Applied Mechanics, SB RAS, Novosibirsk 630090, Russia; alexgol@itam.nsc.ru (A.A.G.); smalik@ngs.ru (A.G.M.)
 - ⁴ Faculty of Mechanical Engineering and Technologies, Novosibirsk State Technical University, Novosibirsk 630073, Russia; e.kornienko@corp.nstu.ru
 - ⁵ Laboratory of Optical Materials and Structures, Institute of Semiconductor Physics, SB RAS, Novosibirsk 630090, Russia
 - ⁶ Research and Development Department, Kemerovo State University, Kemerovo 650000, Russia
 - ⁷ Department of Industrial Machinery Design, Novosibirsk State Technical University, Novosibirsk 630073, Russia
 - ⁸ R&D Center "Advanced Electronic Technologies", Tomsk State University, Tomsk 634034, Russia
- * Correspondence: atuchin@isp.nsc.ru

Abstract: Laser processing is an effective post-treatment method for modifying the structure and improving the properties of cold-sprayed coatings. In the present work, the possibility of fabricating a hard and wear-resistant Ti-based cermet coating by cold spray followed by laser remelting was studied. A mixture of titanium and chromium carbide powders in a ratio of 60/40 wt.% was deposited by cold spray onto a titanium alloy substrate, which ensured the formation of a composite coating with a residual chromium carbide content of about 12–13 wt.%. The optimal values of laser beam power (2 kW) and scanning speed (75 mm/s) leading to the qualitative fusion of the coating with the substrate with minimal porosity and absence of defects were revealed. The microstructure and phase composition of as-sprayed and remelted coatings were examined with SEM, EDS and XRD analysis. It was shown that the phase composition of the as-sprayed coating did not change compared to the feedstock mixture, while the remelted coating was transformed into a β -Ti(Cr) solid solution with uniformly distributed nonstoichiometric TiC_x particles. Due to the change in microstructure and phase composition, the remelted coating was characterized by an attractive combination of higher microhardness (437 HV_{0.1}) and lower specific wear rate ($0.25 \times 10^{-3} \text{ mm}^3/\text{N} \times \text{m}$) under dry sliding wear conditions compared to the as-sprayed coating and substrate. Laser remelting of the coating resulted in a change in the dominant wear mechanism from oxidative–abrasive to oxidative–adhesive with delamination.

Keywords: cold spray; laser remelting; composite coating; titanium; chromium carbide; titanium carbide; microhardness; wear resistance



Citation: Shikalov, V.S.; Katanaeva, D.A.; Vidyuk, T.M.; Golyshev, A.A.; Kosarev, V.F.; Kornienko, E.E.; Malikov, A.G.; Atuchin, V.V. Microstructural Modification of Cold-Sprayed Ti-Cr₃C₂ Composite Coating by Laser Remelting. *J. Compos. Sci.* **2023**, *7*, 500. <https://doi.org/10.3390/jcs7120500>

Academic Editors: Francesco Tornabene and Jinyang Xu

Received: 13 October 2023
Revised: 31 October 2023
Accepted: 29 November 2023
Published: 2 December 2023



Copyright: © 2023 by the authors. Licensee MDPI, Basel, Switzerland. This article is an open access article distributed under the terms and conditions of the Creative Commons Attribution (CC BY) license (<https://creativecommons.org/licenses/by/4.0/>).

1. Introduction

Cold spray is a modern thermal spraying and additive manufacturing method based on the high-velocity impact of solid powder particles (metals, alloys, cermets, polymers) with a substrate at a moderate temperature, which allows for the production of dense coatings while retaining the feedstock phase composition [1–5]. The temperature of gas flow during cold spraying does not exceed the melting point of the feedstock powder. Therefore,

the probability of particle oxidation, decarburization, decomposition, high residual stressing and other negative processes typical for high-temperature thermal spraying methods (HVOF, plasma spraying, detonation spraying) is reduced. Despite the advantages of cold spray, the properties of the as-sprayed coatings are often unsuitable for industrial applications due to their low strength, plasticity, hardness, wear and corrosion resistance. In these cases, to modify the coating properties, various heat treatment techniques are used, such as furnace annealing [6–11], hot isostatic pressing [12–14], spark plasma sintering [15–17], etc.

In recent years, a combined method of cold spraying with subsequent laser treatment has actively been developed. It is worth noting that the Laser-Assisted Cold Spray (LACS) method [18], developed using a combination of these techniques, is currently being developed alongside traditional laser-based additive manufacturing methods [19]. In [20–26], the prospects of laser post-processing for modifying the structure and properties of metal-based cold-sprayed coatings were reported. Sova et al. [20] showed that laser remelting of a 316L coating can significantly reduce its porosity and improve its corrosion resistance. Z. Zhing et al. [21] also showed a similar porosity and corrosion resistance behavior in an aluminum coating after laser treatment. Poza et al. [22] reported a change in the structure of Inconel-625 from lamellar for the as-sprayed coating to columnar dendritic for the remelted coating, resulting in a reduction in hardness but a growth in elastic modulus. Stutzman et al. [23] were able to optimize laser processing parameters to prevent stress corrosion cracking in an alloy 600 coating. Zybala et al. [24] reported both a growth in microhardness and surface hydrophilicity and an increase in residual stresses of titanium and Ti64 alloy coatings after laser treatment. Laser processing is also used to produce alloys from coatings fabricated using metal powder mixtures [25–27]. The multicomponent coating is treated by a laser beam, which induces the melting of precursors. The coating is transformed into a liquid, and solid solutions are formed upon fast cooling and solidification of the melt. N. Kang et al. [25] successfully used laser remelting to prepare a hypoeutectic Al-Si alloy coating with lower roughness and improved hardness compared to the as-sprayed deposit. Sova et al. [26] conducted the first feasibility studies on the application of laser remelting to cold-sprayed multicomponent Cu-Al-316L-Tribaloy 700 and Al-Ti-316L-Tribaloy 700 coatings to produce high-entropy alloys. Similar studies were also performed later in [27] for Fe-Ni-Cu-Co-Al detonation sprayed coatings.

Of particular interest is the laser post-treatment of cold-sprayed cermet coatings, which allows for a significantly enhancement of their mechanical and tribological performance due to the in situ synthesis of new hardening phases [28–32]. Baiamonte et al. [28] compared heat treatment in furnace and laser treatment of a Ti-WC cold-sprayed coating. Laser exposure of the coating led to a decarburization of WC followed by the synthesis of a new phase of TiC, while furnace annealing did not change the phase composition. The formation of a TiC phase resulted in a significant increase in microhardness, decrease in wear rate and a change in wear mechanism compared to the as-sprayed and annealed coating. Goral et al. [29] used laser irradiation to modify the near-surface layer of the composite Cr₃C₂-NiCr-Ni-C coating. With increasing radiation power, Cr₇C₃ and Cr₂O₃ phases were formed in the coating, and residual stresses rose. The change in structure and phase composition led to a growth in microhardness and elastic modulus compared to the as-sprayed coating. In our previous works [30–32], a combined technique of cold spray and laser post-treatment was used to produce multilayer cermet materials using powder mixtures of Ni-B₄C, Ti-B₄C and Ti-WC. The obtained thick deposits showed an improvement in microhardness and high-velocity impact resistance compared to the as-sprayed coatings and substrate.

The present work continues our previous research and aims at the application of a combined method based on cold spray and laser post-treatment to produce hard and wear-resistant composite coatings. The goal of the present work is to study the effect of laser remelting on the microstructure, microhardness and dry sliding wear performance of the coating produced by cold spraying of a Ti-Cr₃C₂ powder mixture. Titanium is a ductile metal which has a high strength-to-weight ratio and excellent corrosion resistance. Chromium carbide (Cr₃C₂) is a hard and wear-resistant ceramic compound. The features

of the interaction between titanium and chromium carbide were considered for composites produced with the sintering [33], casting [34] and electro-spark deposition [35] techniques. In [33], the authors noted that Cr_3C_2 is one of the most suitable additives for strengthening titanium using the powder metallurgy method. Strengthening is achieved by in situ synthesized TiC particulate, Ti(Cr) solid solution and grain refining. In [34], the effect of Cr_3C_2 content on the structure and mechanical properties of cast Ti-matrix composites was studied. Depending on the starting Cr_3C_2 content, the morphology of the synthesized TiC particulate changed in the obtained composites, which allowed for different combinations of enhanced mechanical characteristics (strength and ductility or hardness and toughness). In [35], Ti-Cr-TiC- Cr_7C_3 coatings were obtained by exposing a mixture of Ti granules and Cr_3C_2 powder to electric discharges. The obtained coatings showed increased microhardness (up to 3.5 times), wear resistance (up to 107 times) and heat resistance (up to 3 times) compared to the Ti64 substrate. At the same time, the influence of laser radiation on the structure and properties of Ti- Cr_3C_2 composites has not been investigated yet, which confirms the novelty of the present study. It is known that titanium and titanium alloys have low hardness and poor wear resistance, which limits their use in many applications. For this reason, titanium products require the improvement of surface properties. As a result of laser remelting of Ti- Cr_3C_2 composition, it is possible to form a structure consisting of a solid solution reinforced with hardening particulates. The chosen approach is promising for increasing the hardness and wear resistance of the coating. The obtained coatings may have potential as protective layers on titanium alloy surfaces and are in demand in the aerospace, marine, chemical and biomedical industries.

2. Materials and Methods

Commercial titanium (PTOM-1 grade, NPF, Moscow, Russia) and chromium carbide (MP Kompleks, Izhevsk, Russia) powders were used as starting powders for cold spraying. The average particle sizes measured with a laser diffraction analyzer LS 13 320 (Beckman Coulter, Brea, CA, USA) were $15.6 \mu\text{m}$ ($d_{10} = 2.4 \mu\text{m}$, $d_{90} = 35.3 \mu\text{m}$) and $27.9 \mu\text{m}$ ($d_{10} = 2.8 \mu\text{m}$, $d_{90} = 77.7 \mu\text{m}$) for titanium and chromium carbide powders, respectively. SEM images of the powder particles are given in Figure 1. Ti- Cr_3C_2 homogenous powder mixture at a ratio of 60/40 wt.% was prepared in a V-mixer Venus FTLMV-02 (FILTRA VIBRACION S.L., Badalona, Spain) for 30 min.

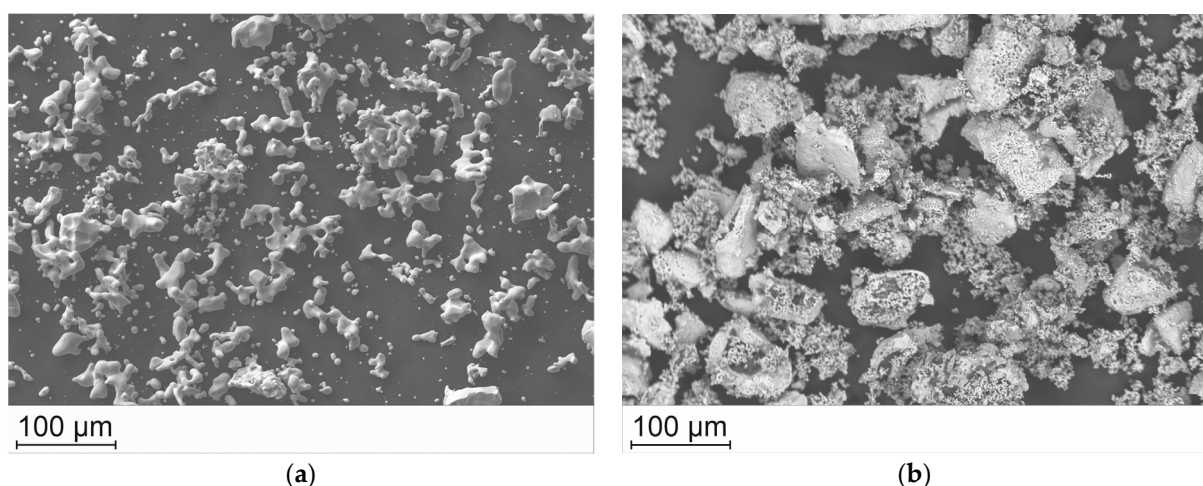


Figure 1. Titanium (a) and chromium carbide (b) powders used for cold spraying.

The mixture was sprayed onto titanium alloy substrates (VT20 grade of Ti-Al-Zr-Mo-V system) with a diameter of 40 mm and a thickness of 8 mm. Prior to spraying, the substrates were grit-blasted with alumina abrasives with an average size of about $300 \mu\text{m}$.

The coatings were deposited on a custom high-pressure cold spray facility (ITAM SB RAS, Novosibirsk, Russia) equipped with an axisymmetric de Laval nozzle OUT1

(Impact Innovations GmbH, Rattenkirchen, Germany). Compressed air was used as the accelerating and carrier gas. The stagnation pressure and temperature were 4 MPa and 400 °C, respectively. The nozzle was moved relative to the substrate at a speed of 100 mm/s at a standoff distance of 30 mm. The pitch between the coating tracks was 3 mm. With the selected cold spraying parameters, a coating thickness of about 600 µm was reached in 2 passes. The as-sprayed coatings were ground to a uniform thickness of about 450 µm to avoid the effect of surface waviness on the following remelting process.

Laser post-processing of coatings was conducted on the automated laser technological complex Siberia 5 (ITAM SB RAS, Novosibirsk, Russia) equipped with a fiber laser (IPG Photonics, Oxford, MI, USA) with a radiation wavelength of 1.07 µm. Laser radiation was focused at a distance of 50 mm above the surface using a lens with a focal length of 300 mm. The diameter of the processed spot on the coating surface was approximately 2.4 mm. Optimization of laser processing parameters was based on the results of our previous works [30,31] and consisted of varying the laser power in the range from 0.5 to 2 kW and the scanning speed from 20 to 100 mm/s when processing single tracks. After finding the optimal mode in terms of absence of macrodefects, the entire coating area was treated in a unidirectional motion mode with a track pitch of 1.2 mm. Laser treatment was carried out in an Ar atmosphere.

Cross-sections of the coatings were mounted into phenolic resin using a hot press Mecapress 3 (Presi, Eybens, France) and polished using an automatic polishing machine Mecatech 334 (Presi, Eybens, France). The microstructure of the coatings' cross-sections and the morphology of the worn surfaces were examined using a scanning electron microscope (SEM) EVO MA15 (Zeiss, Oberkochen, Germany) coupled with an energy-dispersive spectrometer (EDS) X-Max 80 mm² (Oxford Instruments, Abingdon, UK).

X-ray diffraction (XRD) patterns of the powder mixture and coatings surface were recorded by means of an D8 ADVANCE diffractometer (Bruker AXS, Karlsruhe, Germany) with CuK α -radiation. Qualitative XRD analysis was performed using the ICDD PDF-2 (2004) database.

Microhardness was measured according to ASTM E384 on cross-sections using a Tukon 1102 microhardness tester (Wilson, Arnsberg, Germany) via the Vickers method at a constant load of 100 g. The reported microhardness values were averaged from 12 measurements.

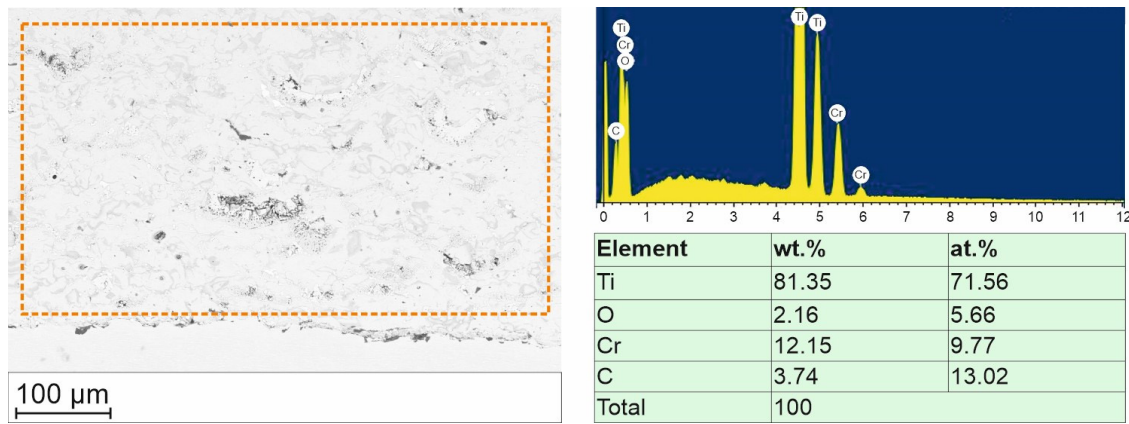
Dry sliding wear tests of the coatings were performed on an UMT-2 tribometer (Bruker Nano, Karlsruhe, Germany) in a ball-on-flat mode according to ASTM G133 with a stroke length of 5 mm, a frequency of 5 Hz and a load of 25 N. The WC-6Co ball with a diameter of 6.35 mm was used as a counterpart. The test time was 2000 s, which is equivalent to a total distance of 100 m. Prior to the tests, the coating surfaces were ground and polished. After the tests, volume loss was measured on 3D profiles obtained with a ContourGT-K1 interference profilometer (Bruker Nano, Karlsruhe, Germany). For each specimen, 3 tests were made, and the average values of coefficient of friction and volume loss were determined. The average value of specific wear rate was calculated as the ratio of volume loss to the product of applied normal load and total sliding distance.

3. Results and Discussion

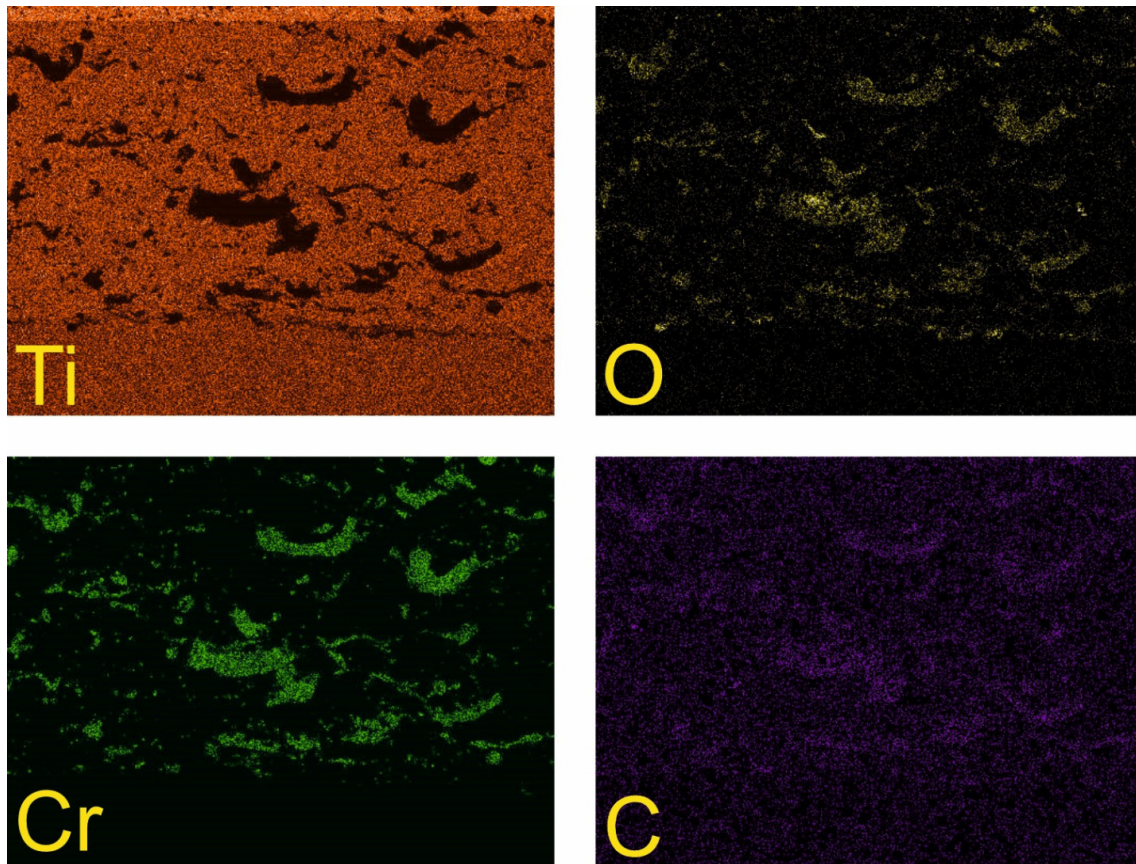
3.1. SEM and EDS Analysis

With the cold spraying parameters and mixture composition used, coatings were successfully deposited onto titanium alloy substrates for further study of their structure and properties. A SEM image of the as-sprayed (AS) coating cross-section and the results of EDS analysis are shown in Figure 2a. Microscopy observation of the coating did not reveal any cracks or other macrodefects. No evidence of the coating delaminating from the substrate was found. The results of the EDS analysis at a standard sensitivity showed that titanium, chromium, oxygen and carbon were found in the coating. It can be seen that the coating composition is different from that of the feedstock powder mixture. It should be noted that, as carbon is a lightweight element, it was quite difficult to obtain reliable

information on its content. Taking this into account, the content of chromium carbide in the coating was estimated as 12–13 wt.%, which is much lower than in the starting mixture. This feature is typical of cold-sprayed powder mixtures consisting of a soft and a hard component, due to the low deposition efficiency of hard particles [36–38]. Elemental maps (Figure 2b) show that chromium carbide particles of various sizes are uniformly distributed in the titanium matrix of the coating. Also note that oxygen in the coating was mainly concentrated on the ceramic particles. To find out the reasons for this, EDS analysis of the chromium carbide powder was performed, which also revealed the presence of oxygen in the particles. This fact may be related to the manufacturing process of the powder.



(a)



(b)

Figure 2. Microstructure of the AS coating cross-section and corresponding EDS results obtained from the area highlighted by the rectangle (a); elemental maps (b). Image was obtained by SEM; maps were obtained by EDS.

In the next step, the cold-sprayed coating was processed with laser irradiation. During laser processing, the focused laser beam moved relative to the specimen, heating the coating material. Thus, in the zone where the laser beam impacted the surface, the coating material melted and a molten pool was formed, which solidified during subsequent cooling. The features of molten pool formation and consequently the structure of the processed material depend on a number of laser processing parameters, such as radiation power, beam diameter, focus position, scanning speed, etc. [28,31]. In the present work, the optimization of laser exposure was performed by varying combinations of laser beam power and scanning speed. Preliminary optical microscopy analysis of the remelted single tracks revealed the optimal values of power (2 kW) and scanning speed (75 mm/s), resulting in quality fusion of the coating with the substrate with minimal porosity and lack of defects (cracks, delamination, etc.). Thus, this mode was chosen for further remelting of the entire coating surface and a detailed examination of its structure and properties.

The SEM image of the laser-processed (LP) coating cross-section and the results of EDS analysis are given in Figure 3. The boundary between the remelted coating and the substrate is clearly visible. The treated coating is characterized by a dense structure consisting of a matrix (light gray) and fine particles (dark gray) uniformly distributed in it (Figure 3a). Most of the synthesized particles of 1–3 μm in size are irregular in shape (Figure 3b), but local aggregations of dendritic particles (Figure 3c) are also observed. The dendritic particles do not show any preferential orientation along the processing direction. A similar hybrid structure was observed for the cast [34] and electro-spark deposited [35] composites. According to EDS data (Figure 3d), the matrix consisted mainly of titanium and chromium, while the particles contained titanium and carbon. Quantitative elemental analysis suggested the formation of the following phases: Ti(Cr) solid solution for the matrix, and TiC_x (where $0 < x < 1$) for irregular and dendritic particles. No substrate-alloying elements (Al, Zr, Mo, V, etc.) were detected in the coating volume, indicating fusion and mixing with the substrate in a thin interface layer. Furthermore, coarse irregular particles (black) were found near the interface, which, according to the results of elemental analysis, were alumina. On the one hand, fine alumina particles could have been retained on the substrate surface after grit-blasting treatment. On the other hand, alumina could have formed as a result of the reaction between aluminum, which is a major alloying element of the titanium alloy substrate, and the oxygen contained in the AS coating. This hypothesis was confirmed by the absence of oxygen in the LP coating. Note that in our previous work [31], a small amount of aluminum was intentionally admixed into a Ti-B₄C coating to absorb oxygen in the molten pool during laser treatment. Some round-shaped pores were also found in the interface zone. The formation of pores can be attributed to the coalescence of smaller pores initially present in the AS coating [25], as well as to the peculiarities of the convective motion of the melt [30].

3.2. XRD Analysis

The results of XRD analysis of the feedstock powder mixture and coatings are shown in Figure 4. It can be seen that the reflections corresponding to the α -Ti (PDF number 44-1294 [39]) and Cr_3C_2 (PDF number 35-804 [40]) phases are observed in the XRD patterns of the powder mixture and the AS coating. After spraying, the phase composition of the coating did not change compared to the feedstock powder mixture, which is typical for the cold spray method. The broadening of the α -Ti and Cr_3C_2 reflections for the AS coating relative to the reflections for the powder indicates a decrease in crystallite size and lattice strain accumulation due to high-velocity impact during the cold spraying process [41]. The TiH_2 (PDF number 78-2216 [42]) and Cr_7C_3 (PDF number 36-1482 [43]) reflections are also observed in the XRD patterns of the powder mixture and the AS coating. They were impurities in the initial Ti and Cr_3C_2 powders, respectively, whose presence was due to the manufacturing process. The low intensity of the TiH_2 and Cr_7C_3 reflections indicates a small quantity of these phases in the material. The presence of TiH_2 and Cr_7C_3 impurities in the titanium and chromium carbide powders, respectively, was confirmed in [44,45].

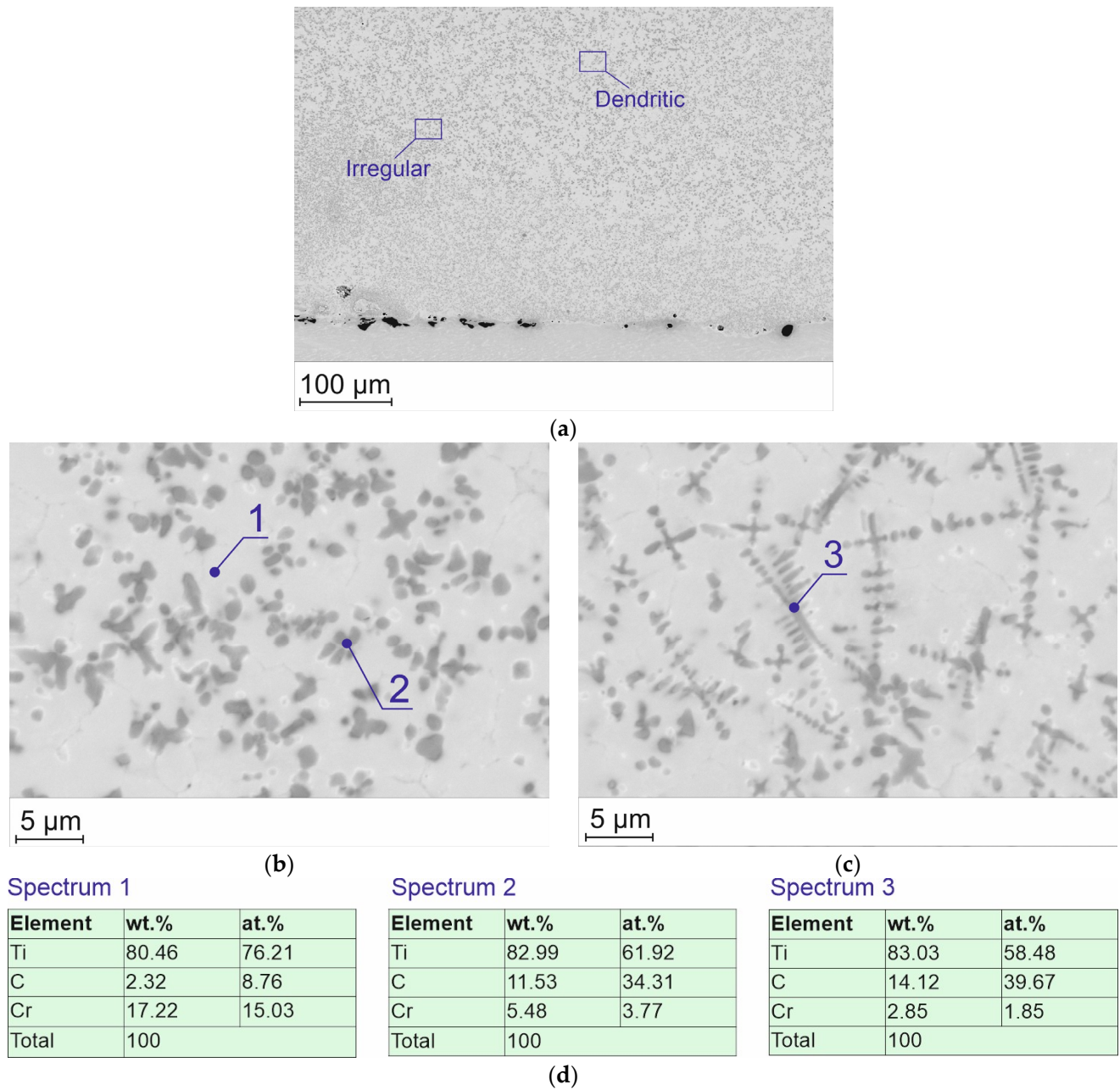


Figure 3. Microstructure of LP coating cross-section at low (a) and high (b,c) magnifications and EDS results (d). Images were obtained by SEM. The LP coating was obtained at a laser power of 2 kW and a scanning speed of 75 mm/s.

The XRD pattern of the LP coating shows the presence of β -Ti (PDF number 65-5970 [46]) and TiC_x (PDF number 32-1383 [47]) reflections. The reflections of the initial α -Ti and Cr_3C_2 phases are absent. Under the impact of laser radiation, chromium carbide particles were dissolved and decarburized in the molten pool. In the Ti-C-Cr system, TiC_x is the more thermodynamically stable chemical compound compared to $TiCr_2$ intermetallic and chromium carbides. For this reason, the TiC_x phase was primarily synthesized as a result of a chemical reaction between titanium and chromium carbides (Equations (1) and (2)) and a reaction between titanium and carbon formed during Cr_3C_2 and Cr_7C_3 dissolution (Equation (3)). The free chromium formed from these reactions was dissolved in the titanium matrix. A metastable solid solution β -Ti(Cr) was formed in the coating due to fast cooling after remelting. The solid solution reflections in the LP pattern are shifted relative to the reflections of pure β -titanium, indicating a change in the lattice parameter of

titanium due to supersaturation with β -stabilizing chromium. The shifting of the reflections of the synthesized TiC_x phase relative to the theoretical data proves its nonstoichiometry.

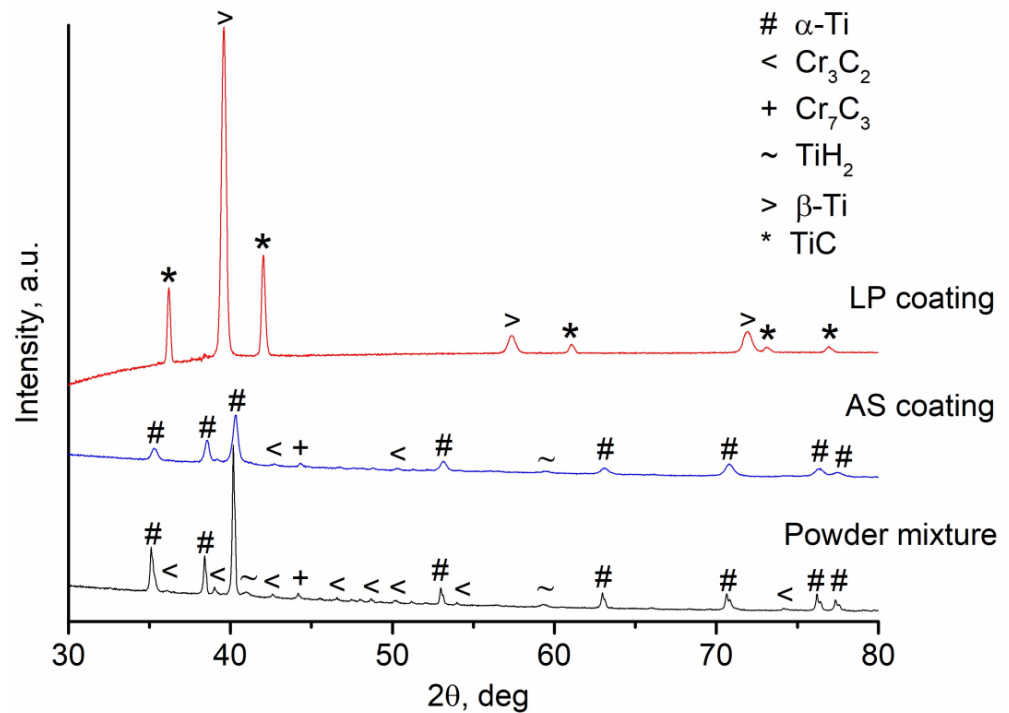


Figure 4. XRD patterns of powder mixture and coatings. The LP coating was obtained at a laser power of 2 kW and a scanning speed of 75 mm/s.

3.3. Microhardness

The results of microhardness measurements are shown in Table 1. Laser processing of the coating resulted in significant growth of coating microhardness, up to 437 $HV_{0.1}$, which is 2.9 times higher than that of the AS coating (151 $HV_{0.1}$) and 1.3 times higher than that of the titanium alloy substrate (341 $HV_{0.1}$). This considerable increase in microhardness is associated with a change in the phase composition of the remelted coating, particularly the formation of a solid solution and the synthesis of the hardening fine particles of titanium carbide [33–35]. Such microhardness behavior of laser-processed cermet coatings was observed in [28–32]. The combination of strengthening mechanisms acts in the laser processed coating in the following ways: solid solution strengthening due to β -Ti(Cr) phase formation, precipitation strengthening due to TiC particles formation and dislocation strengthening due to the thermal expansion mismatch and high cooling rates. In the AS coating, strengthening is preferably provided by cold working due to high-velocity impact during the cold spraying process.

Table 1. Microhardness, specific wear rate and CoFs. The LP coating was obtained at a laser power of 2 kW and a scanning speed of 75 mm/s.

	Microhardness, HV _{0.1}	Specific Wear Rate × 10 ⁻³ , mm ³ /N × m	CoF
Substrate	341.7 ± 7.7	0.4 ± 0.01	0.44 ± 0.003
AS coating	151.4 ± 14.3	1.2 ± 0.04	0.67 ± 0.01
LP coating	437.6 ± 14.2	0.25 ± 0.01	0.7 ± 0.008

3.4. Tribological Characteristics

The results of tribological characterization are presented in terms of specific wear rate, coefficient of friction (CoF) and observation of the worn surface by SEM, EDS and interference profilometry. The results of measurements of specific wear rates and CoFs are listed in Table 1. The LP coating demonstrated the lowest specific wear rate, which was 4.8 times lower than that of the AS coating and 1.6 times lower than that of the substrate. Note that, if we compare microhardness and specific wear rate, a clear inverse correlation is observed. In other words, the higher the microhardness of the material, the lower its specific wear rate. The reduction in specific wear rate in the LP coating is due to the formation of new phases affecting overall microhardness and, consequently, the wear mechanisms.

Different mechanisms, including abrasive, adhesive, oxidative, etc., and their combinations, can act on sliding wear behavior of metal matrix cold-sprayed coatings [48]. Analysis of the AS coating's scar morphology by SEM (Figure 5) showed the presence of grooves parallel to the sliding direction. EDS analysis revealed the presence of a large amount of oxygen (42 at.%), which indicated the formation of oxide films. In the SEM image, the oxide films look like thick, noncontinuous outgrowths. These films crumbled during friction and formed abrasive particles, which led to more intense wear. Thus, the dominant factor of AS coating wear was the oxidative–abrasive mechanism. Examination of the scar morphology of the LP coatings revealed evidence of an adhesive wear mechanism. Signs of adhesion and delamination of the coating material were detected on the worn surface. In addition, tungsten was found on the worn surface (0.16 at.%), indicating mass transfer of the counterpart material into the friction zone. The amount of oxygen on the worn surface of the LP coating was about half as much as on that of the AS coating (24 at.%). Apparently, the growth rate of oxide films on the LP coating was lower than that on the AS coating. The low thickness of the formed oxide films did not lead to their destruction during friction and formation of abrasive particles, but rather acted as a tribolayer and prevented further wear. It can be suggested that this change in phase composition after remelting improved the oxidation resistance of the coating. Analysis of the worn surface morphology by interference profilometry (Figure 6) showed that a small amount of material was plastically displaced from the friction zone to the periphery in the LP coating. At the same time, no material displacement was observed in the AS coating, indicating a brittle fracture of the material in the friction process. Thus, plastic deformation was also slightly involved in the wear process of the LP coating. Summarizing the observations made, it can be concluded that laser treatment resulted in a change in the dominant wear mechanisms, from an oxidative–abrasive mechanism in the AS coating to an oxidative–adhesive mechanism with delamination in the LP coating.

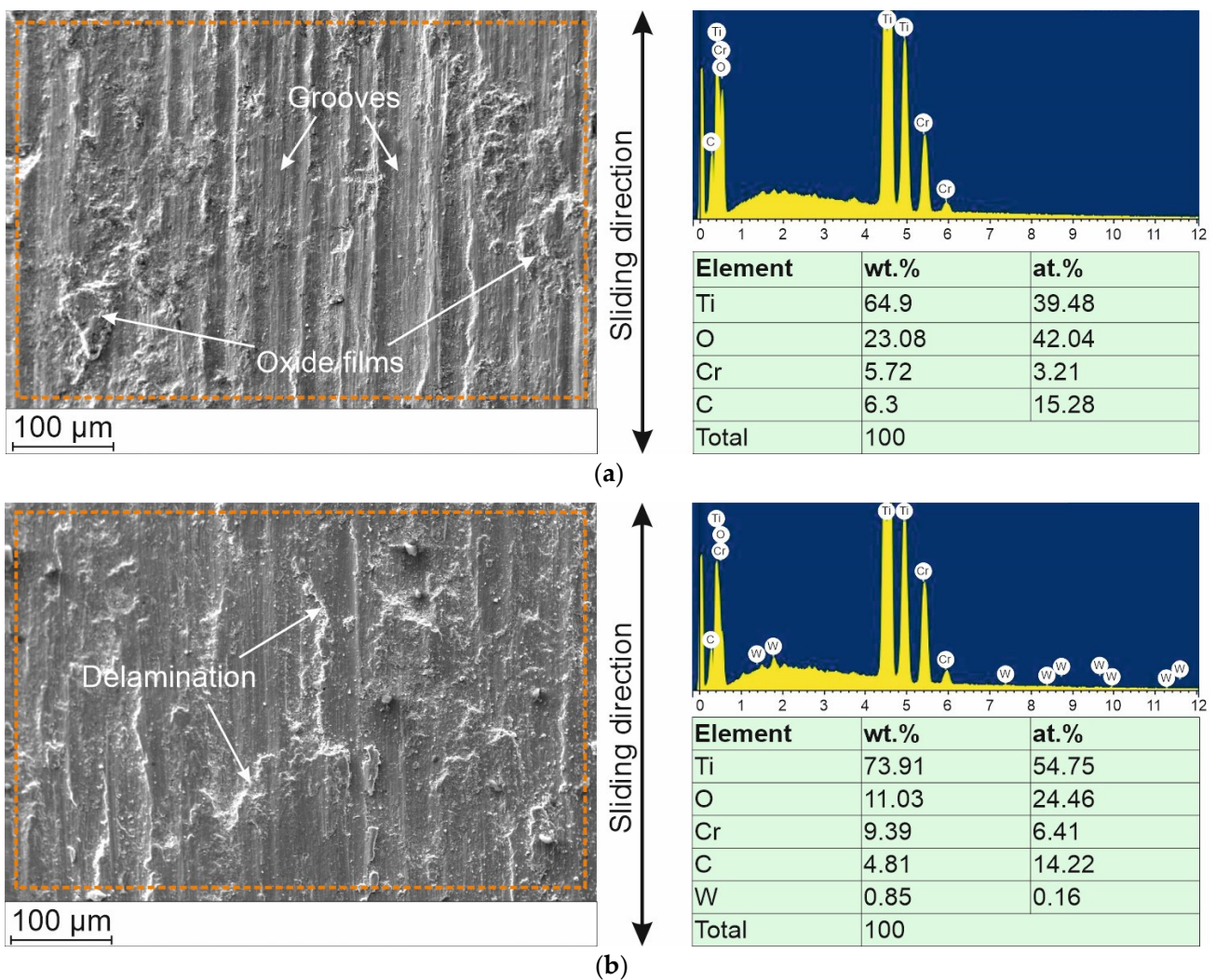


Figure 5. Morphology of worn scars and corresponding EDS results obtained from the area highlighted by the rectangle: (a) AS coating, (b) LP coating. Images were obtained by SEM. The LP coating was obtained at a laser power of 2 kW and a scanning speed of 75 mm/s.

The coefficients of friction (CoFs) are shown in Figure 7 as functions of test time. Average values are given in Table 1. All CoF curves were characterized by a rapid running-in stage (less than 200 s), after which the CoF reached a steady state. The lowest average CoF of 0.44 was observed for the substrate. The average CoF values for the AS and LP coatings were significantly higher, and they were 0.67 and 0.7, respectively. The CoF curve for the LP coating reached a plateau-like trend after 800 s and maintained it for the whole test time. At the same time, the CoF curve for the AS coating after the running-in stage showed a lower level and a slightly increasing trend until the end of the test, when it reached comparable value with the LP coating. As mentioned above, in the present work, the dominant wear mechanism for the AS coating was oxidative wear accompanied by the destruction of thick oxide films and the formation of abrasive particles. The abrasive particles formed during the friction process led to a decrease in the friction force and, accordingly, a gradual increase in the CoF. In the case of the LP coating, the thin oxide tribolayer formed after the running-in stage prevented the formation of abrasive particles, which led to a plateau-like trend in the friction coefficient. It is to be expected that with further increases in test duration, the AS coating CoF would continue to rise, while the LP coating CoF would maintain a plateau-like trend. A similar trend of coefficient of friction during long-time tests was observed in [28], but the CoF value for the remelted coating was much lower than that for the as-sprayed coating, which can be explained by the differences

in the composition and structure of the obtained coatings and the wear test conditions compared to the present work.

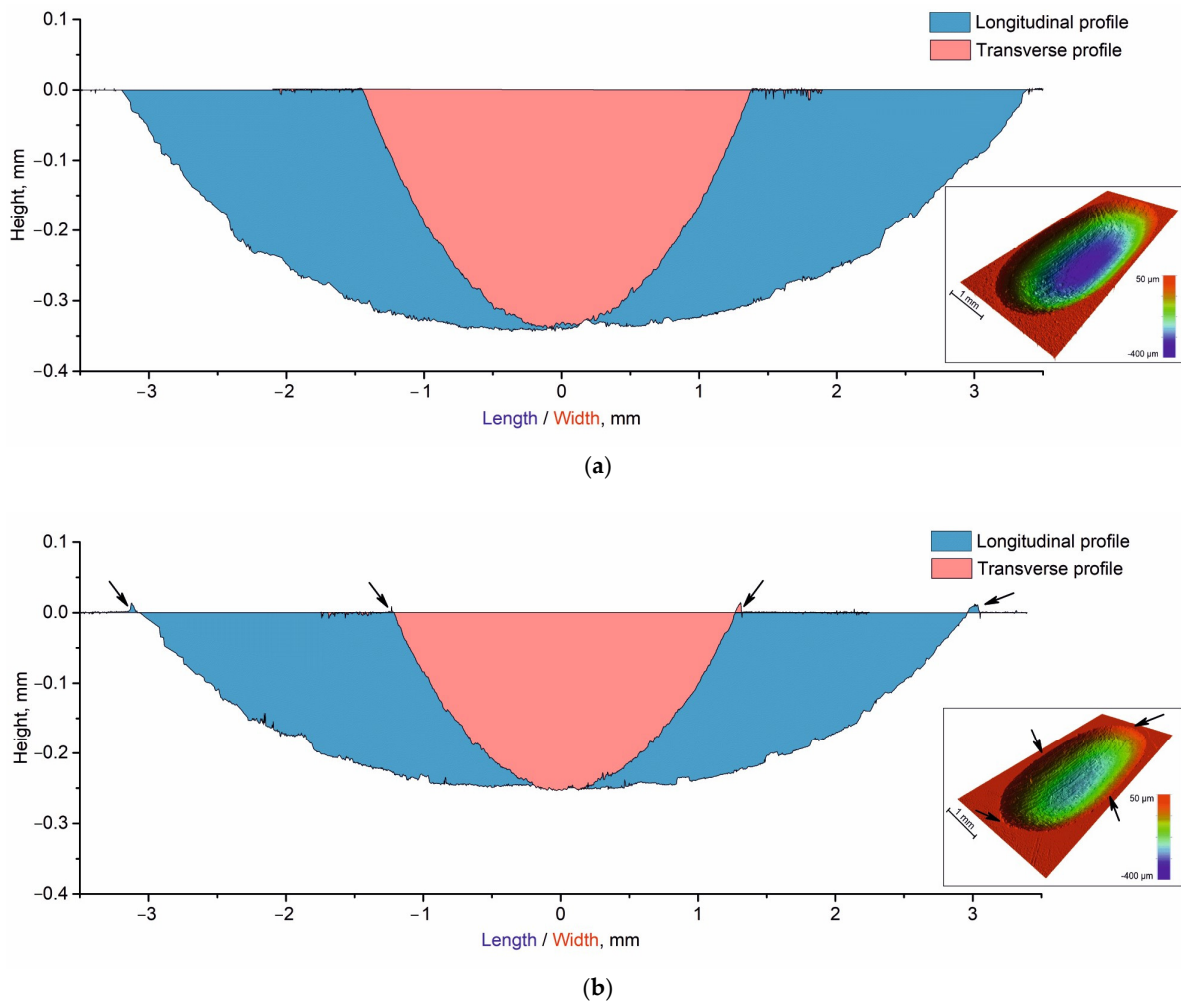


Figure 6. Cross-sectional profiles of worn scars: (a) AS coating, (b) LP coating. Arrows indicate displacement of the coating material from the friction zone. The LP coating was obtained at a laser power of 2 kW and a scanning speed of 75 mm/s.

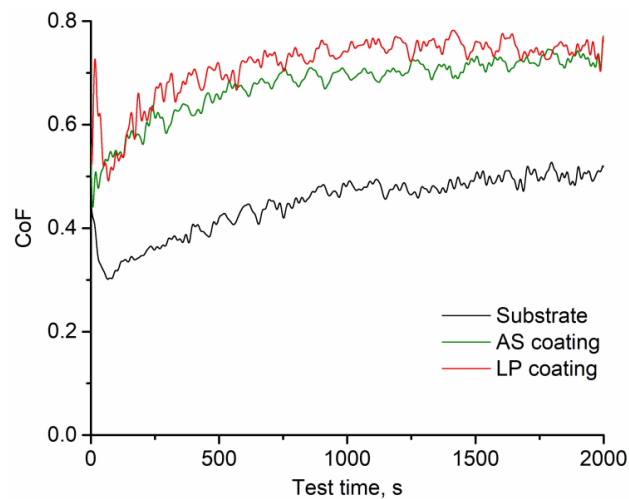


Figure 7. Evolution of CoF during dry sliding wear tests. The LP coating was obtained at a laser power of 2 kW and a scanning speed of 75 mm/s.

4. Conclusions

Using the Ti-Cr₃C₂ powder mixture, composite coatings with a residual Cr₃C₂ content of about 12–13 wt.% were successfully deposited onto titanium alloy substrates by cold spray. The optimal values of laser power (2 kW) and scanning speed (75 mm/s) leading to the qualitative fusion of the coating with the substrate with minimal porosity and absence of defects were revealed. EDS and XRD analyses showed that the phase composition of the as-sprayed coating did not change compared to the feedstock powder, while the laser-treated coating was transformed into a β -Ti(Cr) solid solution with homogeneously distributed irregular and localized dendritic TiC_x particles. Nonstoichiometric TiC_x phases were synthesized as a result of a reaction between titanium and chromium carbides and a reaction between titanium and carbon formed during the dissolution of chromium carbides. A metastable solid solution β -Ti(Cr) formed due to the dissolution of β -stabilizing chromium in the α -titanium matrix and fast cooling after remelting. The remelted coating was characterized by a higher microhardness of 437 HV_{0.1} and a lower wear rate of $0.25 \times 10^{-3} \text{ mm}^3/\text{N} \times \text{m}$ under dry sliding wear conditions compared to the as-sprayed coating and substrate. The wear mechanism changed from oxidative–abrasive for the as-sprayed coating to oxidative–adhesive with delamination for the remelted coating. The obtained results broaden the perspectives for the use of the combined technique of cold spraying with subsequent laser remelting for the fabrication of hard and wear-resistant Ti-based cermet coatings, which are in demand in various modern industrial fields.

Author Contributions: Conceptualization, V.S.S. and A.A.G.; Data curation, V.S.S., D.A.K. and A.A.G.; Funding acquisition, V.S.S.; Investigation, D.A.K., T.M.V. and V.V.A.; Methodology, V.S.S., D.A.K., T.M.V. and A.A.G.; Supervision, V.F.K. and E.E.K.; Writing—original draft, V.S.S. and T.M.V.; Writing—review and editing, V.F.K., E.E.K., A.G.M. and V.V.A. All authors have read and agreed to the published version of the manuscript.

Funding: This work was funded by the Russian Science Foundation, grant number No. 23-29-10123, <https://rscf.ru/project/23-29-10123/> (accessed on 06.03.2023) and the Novosibirsk Region Government.

Data Availability Statement: Data are contained within the article.

Acknowledgments: The study was conducted at the «Mechanics» Equipment Sharing Center of ITAM SB RAS.

Conflicts of Interest: The authors declare no conflict of interest.

References

1. Papyrin, A.; Kosarev, V.; Klinkov, S.; Alkhimov, A.; Fomin, V. *Cold Spray Technology*; Elsevier Science: Amsterdam, The Netherlands, 2007. [[CrossRef](#)]
2. Champagne, V.K. *The Cold Spray Materials Deposition Process. Fundamentals and Applications*; Woodhead Publishing: Cambridge, UK, 2007.
3. Guo, D.; Kazasidis, M.; Hawkins, A.; Fan, N.; Leclerc, Z.; MacDonald, D.; Nastic, A.; Nikbakht, R.; Ortiz-Fernandez, R.; Rahmati, S.; et al. Cold spray: Over 30 years of development toward a hot future. *J. Therm. Spray Technol.* **2022**, *31*, 866–907. [[CrossRef](#)]
4. Vaz, R.F.; Garfias, A.; Albaladejo, V.; Sanchez, J.; Cano, I.G. A review of advances in cold spray additive manufacturing. *Coatings* **2023**, *13*, 267. [[CrossRef](#)]
5. AlMangour, B. Fundamentals of Cold Spray Processing: Evolution and Future Perspectives. In *Cold-Spray Coatings*; Cavaliere, P., Ed.; Springer: Cham, Switzerland, 2018; pp. 3–24. [[CrossRef](#)]
6. Sudharshan Phani, P.; Srinivasa Rao, D.; Joshi, S.V.; Sundararajan, G. Effect of process parameters and heat treatments on properties of cold sprayed copper coatings. *J. Therm. Spray Technol.* **2007**, *16*, 425–434. [[CrossRef](#)]
7. Huang, R.; Sone, M.; Ma, W.; Fukanuma, H. The effects of heat treatment on the mechanical properties of cold-sprayed coatings. *Surf. Coat. Technol.* **2015**, *261*, 278–288. [[CrossRef](#)]
8. Murray, J.W.; Zuccoli, M.V.; Hussain, T. Heat treatment of cold-sprayed C355 Al for repair: Microstructure and mechanical properties. *J. Therm. Spray Technol.* **2018**, *27*, 159–168. [[CrossRef](#)]
9. Chua, A.; Park, C.; Ansell, T.Y.; Nieto, A. Mechanical behavior of annealed cold sprayed Cu-Ni coatings. *J. Therm. Spray Technol.* **2022**, *31*, 574–584. [[CrossRef](#)]
10. Wang, H.; An, F.; Bai, X.; Yao, H.; Zhang, M.; Chen, Q.; Ji, G.; Ramachandran, C.S. Improvement of microstructure and sliding wear property of cold-sprayed FeAl intermetallic compound coating by annealing treatment. *Coatings* **2023**, *13*, 1260. [[CrossRef](#)]

11. Al-Mangour, B.; Mongrain, R.; Irissou, E.; Yue, S. Improving the strength and corrosion resistance of 316L stainless steel for biomedical applications using cold spray. *Surf. Coat. Technol.* **2013**, *216*, 297–307. [[CrossRef](#)]
12. Chen, C.; Xie, Y.; Yan, X.; Yin, S.; Fukanuma, H.; Huang, R.; Zhao, R.; Wang, J.; Ren, Z.; Liu, M.; et al. Effect of hot isostatic pressing (HIP) on microstructure and mechanical properties of Ti6Al4V alloy fabricated by cold spray additive manufacturing. *Addit. Manuf.* **2019**, *27*, 595–605. [[CrossRef](#)]
13. Singh, P.; Singh, H.; Singh, S.; Calla, E.; Grewal, H.S.; Arora, H.S.; Krishnamurthy, A. Development, characterization and high-temperature oxidation behavior of hot-isostatic-treated cold-sprayed thick titanium deposits. *Machines* **2023**, *11*, 805. [[CrossRef](#)]
14. Petrovskiy, P.; Khomutov, M.; Cheverikin, V.; Travyanov, A.; Sova, A.; Smurov, I. Influence of hot isostatic pressing on the properties of 316L stainless steel, Al-Mg-Sc-Zr alloy, titanium and Ti6Al4V cold spray deposits. *Surf. Coat. Technol.* **2021**, *405*, 126736. [[CrossRef](#)]
15. Ito, K.; Ogawa, K. Effects of spark-plasma sintering treatment on cold-sprayed copper coatings. *J. Therm. Spray Technol.* **2014**, *23*, 104–113. [[CrossRef](#)]
16. Vidyuk, T.M.; Dudina, D.V.; Korchagin, M.A.; Gavrilo, A.I.; Bokhonov, B.B.; Ukhina, A.V.; Esikov, M.A.; Shikalov, V.S.; Kosarev, V.F. Spark plasma sintering treatment of cold sprayed materials for synthesis and structural modification: A case study using TiC-Cu composites. *Mater. Lett. X* **2022**, *14*, 100140. [[CrossRef](#)]
17. Liu, Z.; Wang, H.; Wang, Y.; Tian, L.; Li, H.; Liu, W.; He, P.; Liu, H.; Li, R. Comparative study on the annealing of cold-sprayed boron nitride nanosheet/copper coating using spark plasma sintering and atmosphere furnace. *Surf. Coat. Technol.* **2023**, *453*, 129041. [[CrossRef](#)]
18. Olakanmi, E.O.; Doyoyo, M. Laser-assisted cold-sprayed corrosion- and wear-resistant coatings: A review. *J. Therm. Spray Technol.* **2014**, *23*, 765–785. [[CrossRef](#)]
19. AlMangour, B. *Additive Manufacturing of Emerging Materials*; Springer: Cham, Switzerland, 2019. [[CrossRef](#)]
20. Sova, A.; Grigoriev, S.; Okunkova, A.; Smurov, I. Cold spray deposition of 316L stainless steel coatings on aluminium surface with following laser post-treatment. *Surf. Coat. Technol.* **2013**, *235*, 283–289. [[CrossRef](#)]
21. Jing, Z.; Dejun, K. Effect of laser remelting on microstructure and immersion corrosion of cold-sprayed aluminum coating on S355 structural steel. *Opt. Laser Technol.* **2018**, *106*, 348–356. [[CrossRef](#)]
22. Poza, P.; Munez, C.J.; Garrido-Maneiro, M.A.; Vezzu, S.; Rech, S.; Trentin, A. Mechanical properties of Inconel 625 cold-sprayed coatings after laser remelting. Depth sensing indentation analysis. *Surf. Coat. Technol.* **2014**, *243*, 51–57. [[CrossRef](#)]
23. Stutzman, A.M.; Rai, A.K.; Alexandreanu, B.; Albert, P.E.; Sun, E.J.; Schwartz, M.L.; Reutzel, E.W.; Tressler, J.F.; Medill, T.P.; Wolfe, D.E. Laser glazing of cold sprayed coatings for the mitigation of stress corrosion cracking in light water reactor (LWR) applications. *Surf. Coat. Technol.* **2020**, *386*, 125429. [[CrossRef](#)]
24. Zybala, R.; Bucholc, B.; Kaszyca, K.; Kowiorski, K.; Soboń, D.; Żórawski, W.; Moszczyńska, D.; Molak, R.; Pakieła, Z. Properties of cold sprayed titanium and titanium alloy coatings after laser surface treatment. *Materials* **2022**, *15*, 9014. [[CrossRef](#)]
25. Kang, N.; Verdy, C.; Coddet, P.; Xie, Y.; Fu, Y.; Liao, H.; Coddet, C. Effects of laser remelting process on the microstructure, roughness and microhardness of in-situ cold sprayed hypoeutectic Al-Si coating. *Surf. Coat. Technol.* **2017**, *318*, 355–359. [[CrossRef](#)]
26. Sova, A.; Doubenskaia, M.; Trofimov, E.; Samodurova, M. Deposition of high-entropy alloy coating by cold spray combined with laser melting: Feasibility tests. *J. Therm. Spray Technol.* **2022**, *31*, 1112–1128. [[CrossRef](#)]
27. Batraev, I.S.; Ulianitsky, V.Y.; Sova, A.A.; Samodurova, M.N.; Trofimov, E.A.; Pashkeev, K.Y.; Malikov, A.G.; Dudina, D.V.; Ukhina, A.V. A feasibility study of high-entropy alloy coating deposition by detonation spraying combined with laser melting. *Materials* **2022**, *15*, 4532. [[CrossRef](#)]
28. Baiamonte, L.; Pulci, G.; Gisario, A.; Paglia, L.; Marino, A.L.; Tului, M.; Marra, F. WC-Ti coatings deposited via cold gas spray and modified by laser and furnace heat treatments. *J. Therm. Spray Technol.* **2021**, *30*, 2083–2098. [[CrossRef](#)]
29. Goral, A.; Zorawski, W.; Litynska-Dobrzynska, L.; Makrenek, M.; Goly, M.; Trelka, A.; Szlezzynger, M. Laser modification of the microstructure and mechanical properties of (Cr₃C₂-25(Ni₂₀Cr))-5(Ni₂₅C) cermet coatings containing a solid lubricant. *Surf. Coat. Technol.* **2021**, *405*, 126701. [[CrossRef](#)]
30. Fomin, V.M.; Golyshchev, A.A.; Kosarev, V.F.; Malikov, A.G.; Orishich, A.M.; Ryashin, N.S.; Filippov, A.A.; Shikalov, V.S. Creation of heterogeneous materials on the basis of B₄C and Ni powders by the method of cold spraying with subsequent layer-by-layer laser treatment. *J. Appl. Mech. Tech. Phys.* **2017**, *58*, 947–955. [[CrossRef](#)]
31. Fomin, V.M.; Golyshchev, A.A.; Kosarev, V.F.; Malikov, A.G.; Orishich, A.M.; Filippov, A.A. Deposition of cermet coatings on the basis of Ti, Ni, WC, and B₄C by cold gas dynamic spraying with subsequent laser irradiation. *Phys. Mesomech.* **2020**, *23*, 291–300. [[CrossRef](#)]
32. Fomin, V.M.; Golyshchev, A.A.; Malikov, A.G.; Filippov, A.A.; Shikalov, V.S.; Yadrenkin, M.A.; Orishich, A.M. Experimental investigation of the effect of laser treatment on the resistance of a cermet coating to a high-speed impact. *J. Eng. Phys. Thermophys.* **2022**, *95*, 1773–1779. [[CrossRef](#)]
33. Liu, Y.; Chen, L.F.; Tang, H.P.; Liu, C.T.; Liu, B.; Huang, B.Y. Design of powder metallurgy titanium alloys and composites. *Mater. Sci. Eng. A* **2006**, *418*, 25–35. [[CrossRef](#)]
34. Zhang, J.; Yang, Z.; Yang, X.; Jia, X.; Yang, M.; Guo, Y.; Li, J.; Yu, Y. A low-cost and high-performance casted titanium matrix composite with Cr₃C₂ additions. *Mater. Lett.* **2023**, *330*, 133407. [[CrossRef](#)]

35. Burkov, A.A.; Kulik, M.A. Electrospark deposition of coatings using Cr_3C_2 powder and their characterization. *Lett. Mater.* **2019**, *9*, 243–248. [[CrossRef](#)]
36. Fernandez, R.; Jodoin, B. Cold spray aluminum-alumina cermet coatings: Effect of alumina content. *J. Therm. Spray Technol.* **2018**, *27*, 603–623. [[CrossRef](#)]
37. Feng, C.; Guipont, V.; Jeandin, M.; Amsellem, O.; Pauchet, F.; Saenger, R.; Bucher, S.; Iacob, C. $\text{B}_4\text{C}/\text{Ni}$ composite coatings prepared by cold spray of blended or CVD-coated powders. *J. Therm. Spray Technol.* **2012**, *21*, 561–570. [[CrossRef](#)]
38. Alidokht, S.A.; Vo, P.; Yue, S.; Chromik, R.R. Cold spray deposition of Ni and WC-reinforced Ni matrix composite coatings. *J. Therm. Spray Technol.* **2017**, *26*, 1908–1921. [[CrossRef](#)]
39. Sailer, R.; McCarthy, G. *ICDD Grant-in-Aid 1993, JCPDS code 44-1294*; North Dakota State University: Fargo, ND, USA, 1993.
40. Rundquist, S.; Runnsjo, G. Crystal structure refinement of Cr_3C_2 . *Acta Chem. Scand.* **1969**, *23*, 1191–1199. [[CrossRef](#)]
41. Brewer, L.N.; Schiel, J.F.; Menon, E.S.K.; Woo, D.J. The connections between powder variability and coating microstructures for cold spray deposition of austenitic stainless steel. *Surf. Coat. Technol.* **2018**, *334*, 50–60. [[CrossRef](#)]
42. Numakura, H.; Koiwa, M.; Asano, H.; Izumi, F. Neutron diffraction study of the metastable γ titanium deuteride. *Acta Met.* **1988**, *36*, 2267–2273. [[CrossRef](#)]
43. McMurdie, H.F.; Morris, M.C.; Evans, E.H.; Paretzkin, B.; Wong-Ng, W.; Hubbard, C.R. Methods of producing standard X-ray diffraction powder patterns. *Powder Diffr.* **1986**, *1*, 40–43. [[CrossRef](#)]
44. Song, Y.; Qiu, F.; Savvakina, D.; Xu, X.; Stasiuk, O.; Ivasishin, O.; Cheng, T. In situ Ti6Al4V/TiB composites prepared by hydrogen-assisted sintering of blends containing TiH_2 and ball-milled Ti+TiB₂ powders. *Materials* **2022**, *15*, 1049. [[CrossRef](#)] [[PubMed](#)]
45. Batraev, I.S.; Ulianitsky, V.Y.; Shtertser, A.A.; Dudina, D.V.; Ukhina, A.V. Formation of composite coatings during detonation spraying of Cr_3C_2 . *J. Compos. Sci.* **2023**, *7*, 71. [[CrossRef](#)]
46. Schmitz-Pranghe, N.; Duenner, P. Crystal structure and thermal expansion of scandium, titanium, vanadium, and manganese. *Z. Metallkd.* **1968**, *59*, 377–382.
47. National Bureau of Standards (U.S.). *Standard X-ray Diffraction Powder Patterns*; U.S. Government Printing Office: Washington, D.C., U.S.A, 1981; Volume 25, p. 73.
48. He, L.; Hassani, M. A review of the mechanical and tribological behavior of cold spray metal matrix composites. *J. Therm. Spray Technol.* **2020**, *29*, 1565–1608. [[CrossRef](#)]

Disclaimer/Publisher’s Note: The statements, opinions and data contained in all publications are solely those of the individual author(s) and contributor(s) and not of MDPI and/or the editor(s). MDPI and/or the editor(s) disclaim responsibility for any injury to people or property resulting from any ideas, methods, instructions or products referred to in the content.